

Muon Acceleration for Neutrino Factory

V. Lebedev, *Jefferson Lab, Newport News, VA 23693*

A concept for a neutrino factory muon accelerator driver is presented. Acceleration of a muon beam is a challenging task because of a large source phase space and short species lifetime. In the design concept presented here, acceleration starts after ionization cooling at 210 MeV/c and proceeds to 20 GeV where the beam is injected into a neutrino factory storage ring. The key technical issues, beyond the basic physics parameters of Table 1, are: 1) choice of acceleration technology (superconducting versus normal conducting cavities) and related to it RF frequency choice, 2) choice of acceleration scheme, 3) capture, acceleration, transport and preservation of the large source phase space of the fast decaying species, and 4) accelerator performance issues such as potential collective effects (e.g., cumulative beam breakup) resulting from the high peak current. To counteract muon decay the highest possible accelerating gradient is required. That is the major driver for the proposed scheme. The muon accelerator driver (MAD) consists of a 2.87 GeV linac and consecutive four-pass recirculating linear accelerator as shown in Figure 1.

Table 1. Main Parameters of the Muon Accelerator Driver

Injection momentum/Kinetic energy	210/129.4 MeV
Final energy	20 GeV
Initial normalized acceptance	15 mm·rad
rms normalized emittance	2.4 mm·rad
Initial longitudinal acceptance, $\Delta p L_b / m_\mu$	170 mm
momentum spread, $\Delta p/p$	± 0.21
bunch length, L_b	± 407 mm
rms energy spread	0.084
rms bunch length	163 mm
Number of bunches per pulse	67
Number of particles per bunch/per pulse	$4.4 \cdot 10^{10} / 3 \cdot 10^{12}$
Bunch frequency/accelerating frequency	201.25/201.25 MHz
Average repetition rate	15 Hz
Time structure of muon beam	6 pulses at 50 Hz with 2.5 Hz repetition rate
Average beam power	150 kW

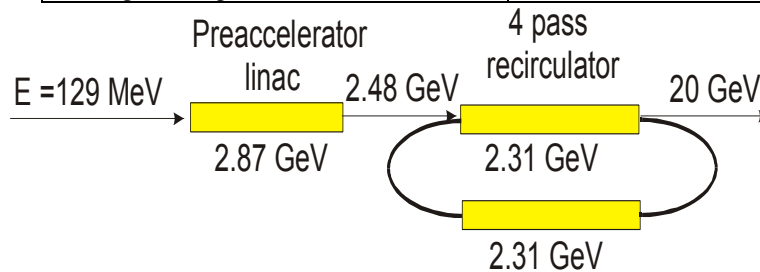


Figure 1. Layout of the muon accelerator driver

Very large transverse and longitudinal accelerator acceptances drive the design to low RF frequency. Were normal-conducting cavities used, the required high gradients of order of ~ 15 MV/m would demand unachievably high peak power of RF sources. Superconducting RF (SRF) cavities are a much more attractive solution. RF power can then be delivered to the cavities over an extended time, and thus RF source peak power can be reduced. Another important advantage of SRF cavities is that their design is not limited by a requirement of low shunt impedance and therefore their aperture can be significantly larger. Taking into account the required longitudinal and transverse acceptances and that the beam is already bunched at 201.25 MHz at the source (ionization cooling) the 201.25 MHz RF-frequency has been chosen for both the linear accelerator and the recirculator. This choice also provides adequate stored energy to accelerate multiple passes of a single-pulse bunch train without need to refill the extracted energy between turns.

Muon survival practically excludes use of conventional circular accelerator and demands either a high-gradient conventional or recirculating linac. While recirculation provides significant cost savings over a single linac, it cannot be utilized at low energy for two reasons. First, at low energy the beam is not sufficiently relativistic and will therefore cause a phase slip for beams in higher passes, thus significantly reducing acceleration efficiency for subsequent passes. Secondly, there are major difficulties associated with injection of a beam with the large emittance and energy spread associated with a muon source. Beam pre-acceleration in a linear accelerator to about 2.5 GeV makes the beam sufficiently relativistic and adiabatically decreases the phase space volume so that further acceleration in recirculating linacs is possible.

Cost considerations favor multiple passes per stage, but practical experience commissioning and operating recirculating linacs dictates prudence. Experience at Jefferson Lab suggests that for

given large initial emittance and energy spread, a ratio of final-to-injected energy below 10-to-1 is prudent and the number of passes should be limited to about five¹. We therefore propose a machine architecture (see Figure 1) featuring a 0.13-to-2.48 GeV straight “preaccelerator” linac, and 2.48-to-20 GeV four pass recirculating linac (RLA). Figure 2 shows loss of muons in the course of acceleration. One can see that although RLA gives significant contribution the major fraction comes from the linac. One can also

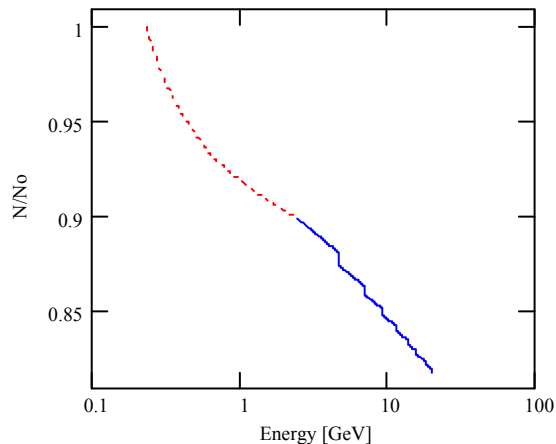


Figure 2. Decay of muons in the course of acceleration; dotted line – decay in the linac, solid line – decay in the recirculator. Vertical drops correspond to the beam transport in arcs.

¹ Note that for given parameters further increase of number of passes reduces effective accelerating gradient and consequently leads to higher decay of muons.

see that arcs (vertical drops in Figure 2) do not contribute much in the decay, which justifies the choice of normal conducting bends, and triplet focusing discussed below.

1. Linear accelerator

1.1 Linac general parameters and lattice period layout

Initial large acceptance of the accelerator requires large aperture and tight focusing at its front-end. In the case of large aperture, tight space, moderate energy and necessity of strong focusing in both planes the solenoidal focusing is superior to the triplet focusing and has been chosen for the entire linac. To achieve a manageable beam size at the linac front-end short focusing cells are used for the first 11 cryo-modules. The beam size is adiabatically damped with acceleration, and that allows one to replace short cryo-modules with intermediate-length cryo-modules and then, when the energy reaches 0.75 GeV by long (standard) cryo-modules. In comparison with the standard 13 m cryo-modules the short and intermediate-length cryo-modules have increased aperture and, consequently, reduced accelerating gradient. Main parameters of the linac and its periods are presented in Tables 2 and 3. Figure 3 depicts the layouts of short, intermediate-length and long cryo-modules. Figures 4 and 5 present the beam envelope and beta-function along the linac.

Table 2. Main parameters of linear accelerator

Injection momentum/Kinetic energy	210 / 129.4 MeV
Final momentum/Kinetic energy	2583 / 2480 MeV
Total linac length	433 m
Acceptance: initial / final (no emittance dilution)	7.5 / 0.62 mm-rad
Momentum spread: initial / final	$\pm 0.21 / \pm 0.075$
Total bunch length: initial / final	814 / 190 mm 197 / 46 deg
Total installed accelerating voltage	2.87 GeV

Table 3. Parameters of the long and short periods of linear accelerator

	Short cryo-module	Intermediate-length cryo-module	Long cryo-module
Number of periods	11	16	19
Total length of one period	5 m	8 m	13 m
Number of cavities per period	1	2	4
Number of cells per cavity	2	2	2
Number of couplers per cavity	2	2	2
Cavity accelerating gradient	15 MV/m	15 MV/m	17 MV/m
Real-estate gradient	4.47 MV/m	5.59 MV/m	7.79 MV/m
Aperture in cavities ($2a$)	460 mm	460 mm	300 mm
Aperture in solenoids ($2a$)	460 mm	460 mm	360 mm
Solenoid length	1 m	1 m	1.5 m
Solenoid maximum field	2.1 T	2.1 T	4.2 T

The layout of cryo-modules and the arrangement of SC cavities are determined by the requirement to keep power of the fundamental coupler at acceptable level and to have cavities sufficiently decoupled. The coupler power limitation (below 1 MW) requires 1 coupler per cell and therefore we choose to have the coupler at each side of two-cell

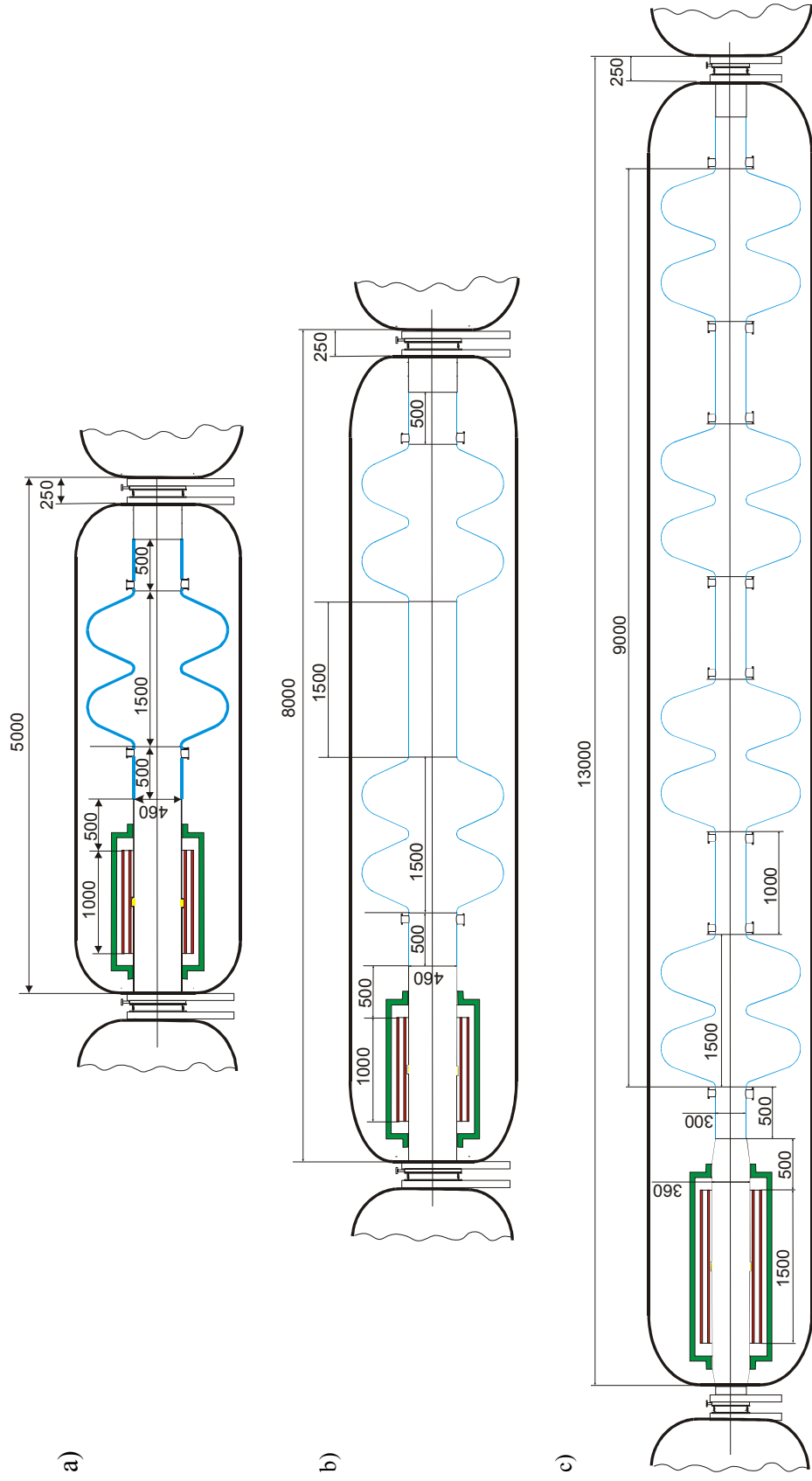


Figure 3. Layouts of a) short, b) intermediate-length, and c) long cryo-modules. Blue lines present SC walls of cavities. Solenoid coils are marked by red color, and BPMs by the yellow.

Fri Feb 23 10:42:26 2001 OptiM - MAIN: - C:\Optics\NeutrinoFactory\Linac\Linac.opt

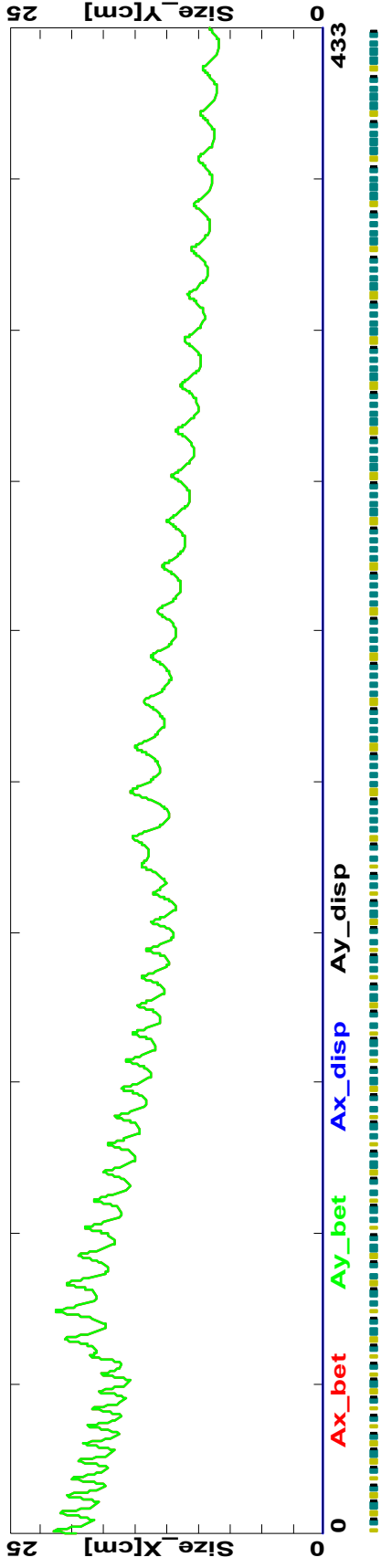


Figure 4. Beam envelopes of the entire beam (2.5σ) along linear accelerator

Fri Feb 23 10:40:52 2001 OptiM - MAIN: - C:\Optics\NeutrinoFactory\Linac\Linac.opt

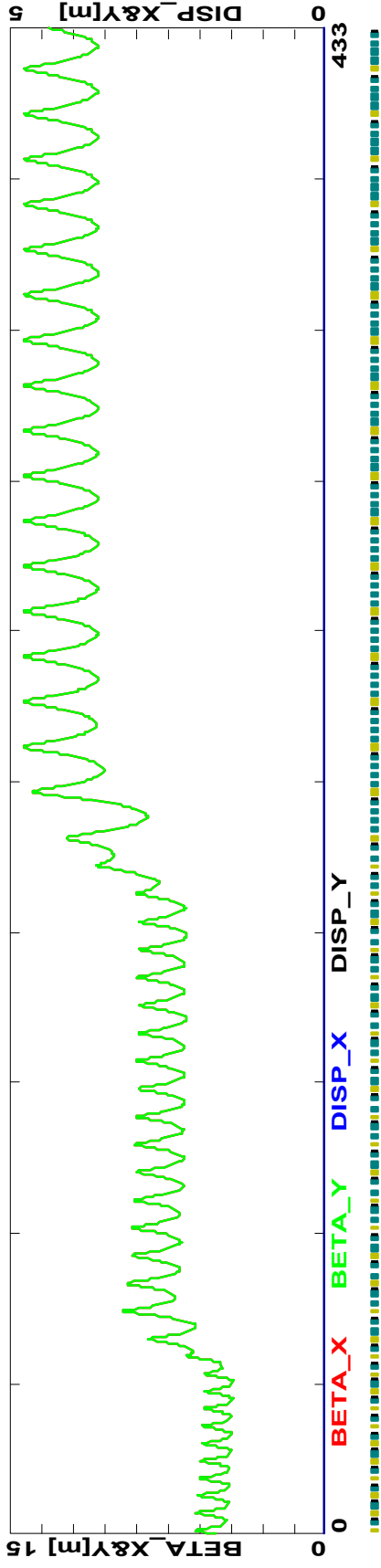


Figure 5. Beta-functions along the linear accelerator. The beta-functions are computed in the frame, which rotates with angular frequency equal to $\omega = eB_s/2pc$ so that the beam motion would be decoupled.

cavity.

The coupling coefficient determined as $\delta = C_3 / C_1$ (see Figure 6) should be sufficiently small,

$$\delta \leq \frac{1}{10Q}, \quad (1)$$

to have a possibility to by-pass not properly functioning cavities. Figure 7 demonstrates effects of cavity coupling and detuning on the cavity voltage. Thus for loaded Q of $5 \cdot 10^5$ the required cavity decoupling should be below $2 \cdot 10^{-6}$.

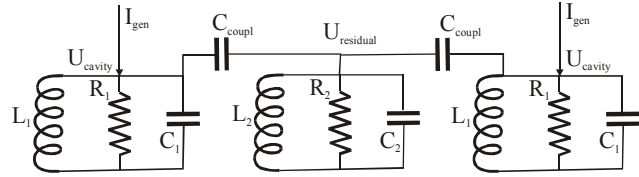


Figure 6. Electrical circuitry for calculation of cavity coupling

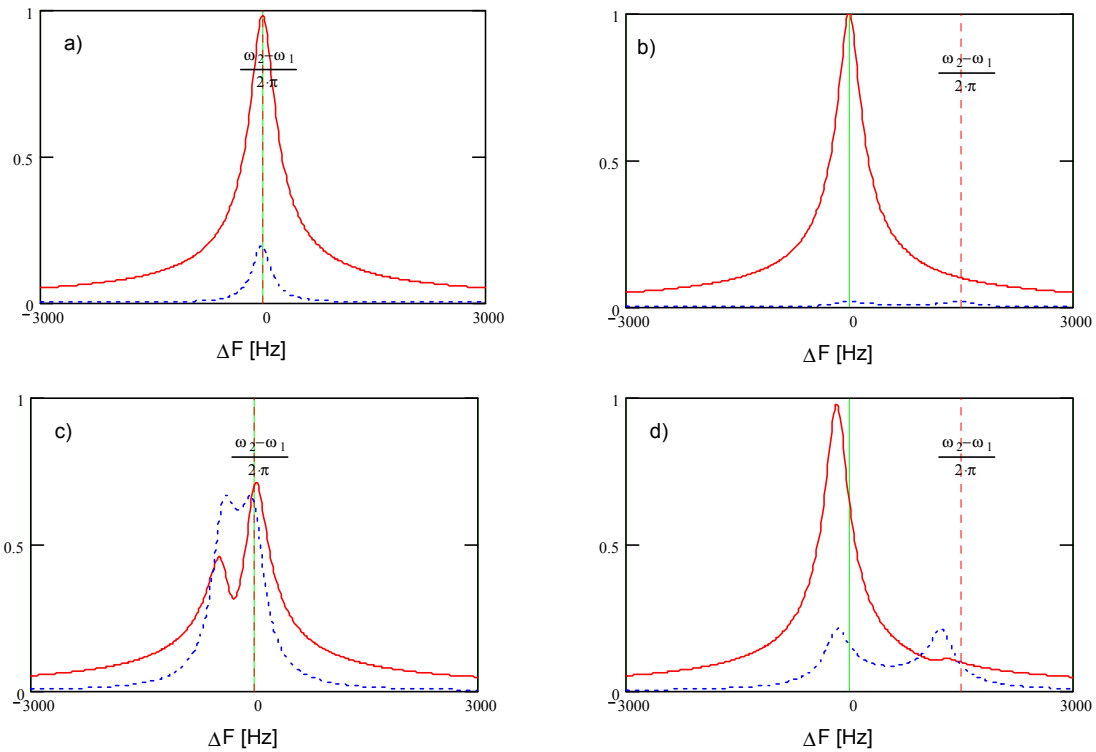


Figure 7. Dependence of cavity voltage on frequency. Solid lines – voltage for normally powered cavity; dashed line – voltage for not properly functioning cavity with corresponding power generator off; a)&c) - cavity is not detuned, b)&d) - cavity is detuned by five bandwidth; a)&b) $\delta = 0.1 / Q$, c)&d) $\delta = 1 / Q$; $Q = 5 \cdot 10^5$.

Such decoupling requires significant distances between nearby cavities. For an estimate one can assume that coupling between cavity cells to be 5%, and then using results presented in Figure 8 one obtains that distance between cavities has to be more than 110 cm for short cry-modules and 70 cm for long cryo-modules. Taking into account that the fundamental and high HOM couplers are located in the same space these distances were chosen to be 150 and 100 cm, correspondingly. BPMs are located inside solenoids to reduce effects of EMI signals coming from RF cavities

There is an additional limitation on the layout of the linac determined by a requirement that all cavities are treated and vacuumed in a clean room and kept under

vacuum all the time after it. That determines that each cryo-module has to have vacuum valves at both ends with corresponding transition modules from liquid helium temperature to the room temperature. To achieve the maximum real-estate accelerating gradient the focusing solenoids are also located inside cryo-modules.

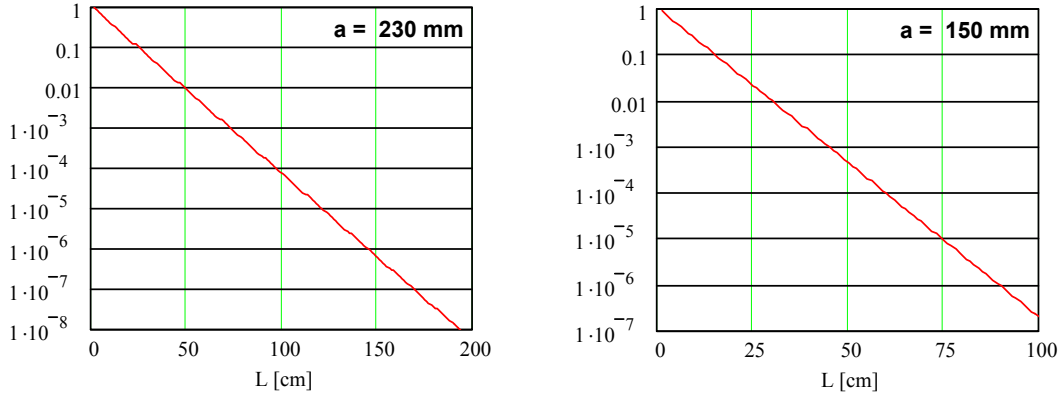


Figure 8. Attenuation of the electromagnetic wave between two cavities for short (left) and long (right) cryo-modules. The attenuation is estimated by the following formula: $\delta = \exp\left(-L\sqrt{(\mu_0 / a)^2 - (2\pi / \lambda)^2}\right)$.

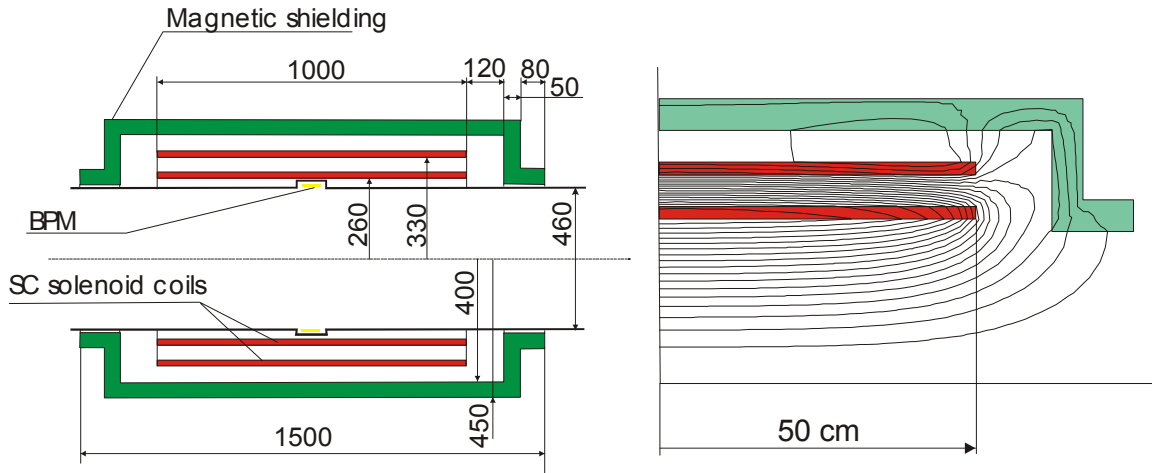


Figure 9. Layout of short solenoid and plot of its magnetic lines

Taking the large aperture required by the beam size the question of solenoids focusing linearity has to be addressed. The dependence of focusing strength on radius can be approximated by the following expression:

$$\Phi \equiv \frac{1}{F} \approx \left(\frac{e}{2pc}\right)^2 \left(\int B^2 ds + \frac{r^2}{2} \int B'^2 ds \right) \approx L \left(\frac{eB_0}{2pc}\right)^2 \left(1 + \frac{r^2}{3aL}\right) \quad , \quad (2)$$

where L and a are the solenoid length and radius. As one can see from Eq. (2) to reduce the non-linearity one needs to increase the solenoid length and aperture. Increasing length directly decreases the real-estate gradient; while increasing aperture requires larger distance between the solenoid and cavity to shield magnetic field and in the final score also decreases real-estate gradient. Aperture increase also makes solenoids more

expensive and less reliable. The length of short solenoid has been chosen to be 1 m as a compromise between these contradictory requirements. The length of long solenoids is determined by the magnetic field limitation and is chosen to be 1.5 m. The layout of the short solenoid and plots of magnetic lines are shown in Figure 9. To achieve fast field drop from solenoid to cavity the solenoid has an outer counter-coil, which intercepts its magnetic flux, and the cavity has a SC shielding at its outer surface. That allows one to achieve magnetic field less than 0.1 G inside the cavity as depicted in Figure 10.

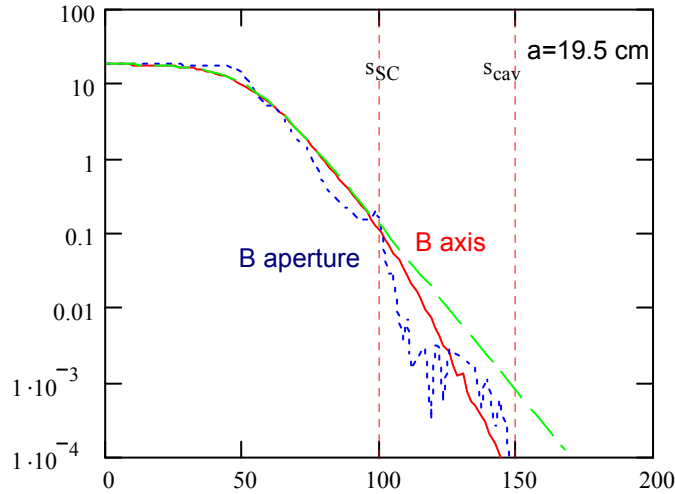


Figure 10. Dependence of magnetic field on longitudinal coordinate: solid line - on the axis, dotted line - on the radius equal to the cavity radius of 23 cm, dashed line - fitting with the following formula: $B(s) = (B_0 / 2)(1 - \tanh((s - L / 2) / a))$, where $a = 19.5$ cm. Vertical lines show positions where the SC screen and cavity start.

1.2 Longitudinal beam dynamics

Initial bunch length and energy spread are very large, so that the bunch length is more than the half wave length ($\Delta\phi = \pm 89$ deg) and the momentum acceptance is about $\pm 21\%$. Therefore their decrease (due to adiabatic damping) to a manageable level is the most important assignment of the beam acceleration in the linac. The final linac energy is also determined by achieving velocity sufficiently close to the light velocity so that there would not be significant RF phase slip for higher passes in the recirculator.

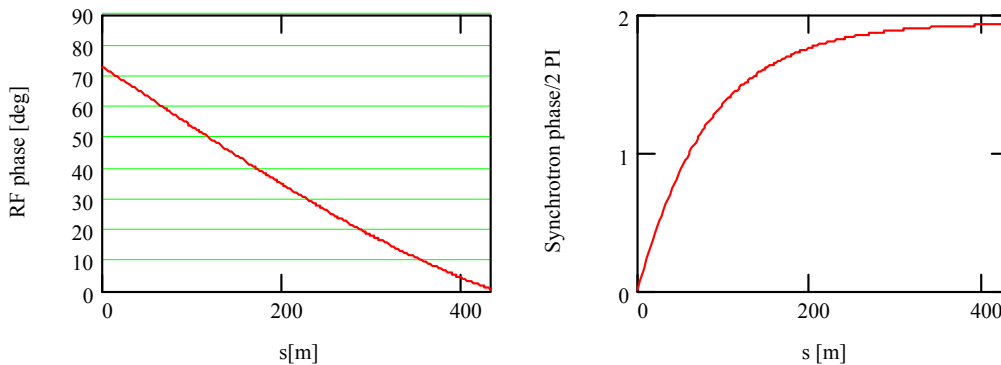


Figure 11. RF (left) and synchrotron (right) phases along the linac.

To perform adiabatic bunching, the RF phase of the cavities is shifted by 73 deg at

the beginning of the linac and is gradually changed to zero at the linac end as shown in Figure 11. In the first half of the linac, when the beam is still not sufficiently relativistic, the offset causes synchrotron motion which prevents the sag in acceleration for the bunch head and tail, and allows bunch compression in both length and momentum spread to $\Delta p/p = \pm 7.5\%$ and $\Delta\phi = \pm 23$ deg but the RF phase offset also reduces effective accelerating gradient so that the total voltage of 2.87 GV is required for the beam acceleration of 2.35 GeV. To maximize longitudinal acceptance its initial position is shifted relative to the center of the bucket. Figure 12 depicts position of the beam boundary inside separatrix; and Figure 13 shows how the initially elliptical boundary of the bunch longitudinal phase space is transformed to the end of the linac.

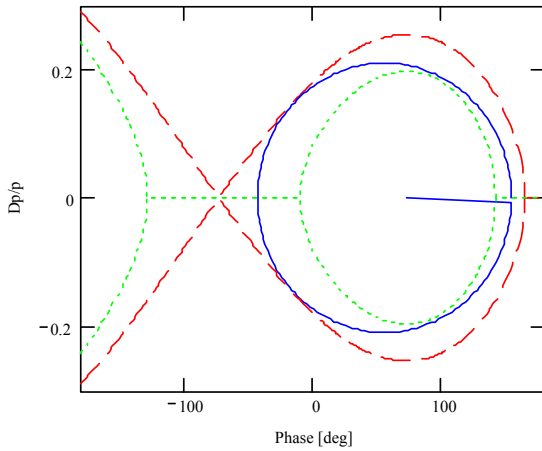


Figure 12. Beam boundary (solid line) inside separatrix (dashed line) shown at the beginning of the linac.

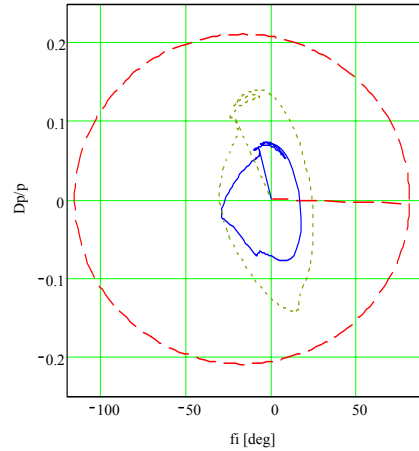


Figure 13. Beam boundary at the beginning (dashed line), in the middle (dotted line) (left) and at the end of the linac

1.3 Transverse beam dynamics and tracking

Betatron phase advance per cell, ν , is important parameter determining properties of the beam transport in the linac. There are a few considerations, which need to be taken into account. First, large beam emittance and limited aperture in the cavities require minimization of the beam size for a given period length. As one can see from Figure 14 it points to ν close to 0.25. Second, one would like to minimize dependence of beta-function variation with momentum. For the same initial conditions the beta-function oscillates relative to its nominal value if momentum is changed. Figure 15 presents ratio of maximum beta-function achieved in the course of oscillations to the maximum of beta-function at equilibrium energy. As one can see for momentum spread of $\pm 20\%$ it requires tunes below 0.25. Third, solenoids are short comparative to the beam aperture

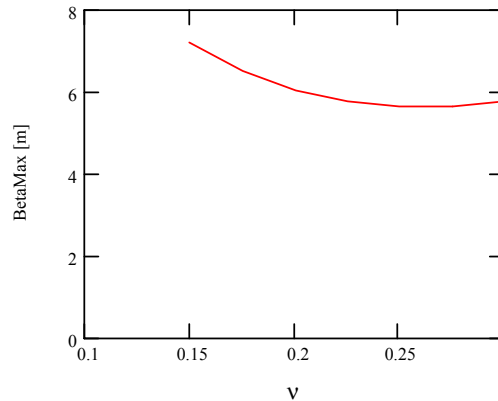


Figure 14. Dependence of maximum beta-function on tune advance per cell for a line with solenoidal focusing and period length 6 m.

and therefore they have significant non-linearity in their focusing. As one can see from Eq. (2) for $a = 19$ cm, $r = 23$ cm and $L=1$ m one obtains correction of focusing strength of 9% at the beam boundary. Such non-linearity can cause strong non-linear resonance even for small number of lattice periods. Figure 16 presents how beam emittance is changing for different phase advances per cell after passing a channel with 50 solenoidal lenses. One can see very strong effect of the $1/4$ resonance which spreads in the tune range of $[0.21 - 0.24]$. The $1/6$ resonance is also well visible but does not produce so harmful effect. In reality it is much smaller because of adiabatic damping of the beam size with acceleration. Taking all above into account we choose tune to be equal to 0.175.

Particle distribution for tracking has been chosen to be Gaussian in 6D phase space but the tails of the distribution are truncated at 2.5σ , which corresponds to the beam acceptance presented in Table 1. Despite the large initial energy spread, particle tracking through the linac does not exhibit any significant emittance growth with 0.2% beam loss coming mainly from particles at the longitudinal phase space boundary. Figure 17 presents longitudinal phase space at the beginning and the end of accelerator. Figure 18 shows the beam emittances and beam envelopes and beam intensity along the linac. Sudden increase and then decrease of the envelopes correspond to a particle motion instability with consecutive particle scraping. The decay of muons is not taken into account in the beam intensity plot.

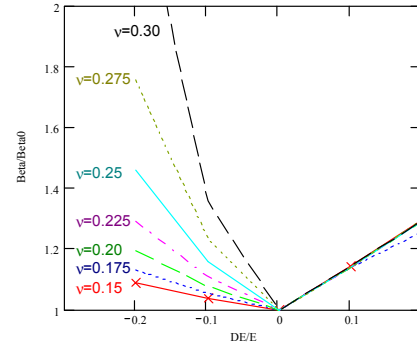


Figure 15. Dependence of relative change of beta-function maximum on relative momentum change for different tune advances per cell.

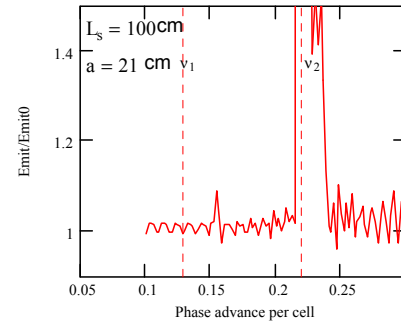


Figure 16. Relative emittance change after passing 50 solenoidal lenses of 1 m length; $\epsilon_n = 15$ mm rad, vertical lines show betatron tune spread in the beam: $\Delta v/v \approx \Delta p/p = \pm 26\%$

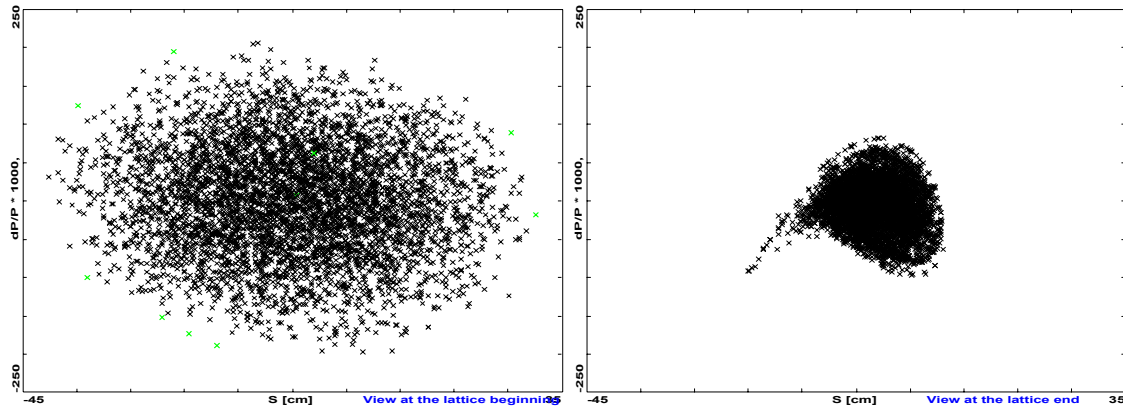


Figure 17. Longitudinal phase space at the beginning (left) and at the end (right) of the linac. Green crosses show particles lost in the course of acceleration.

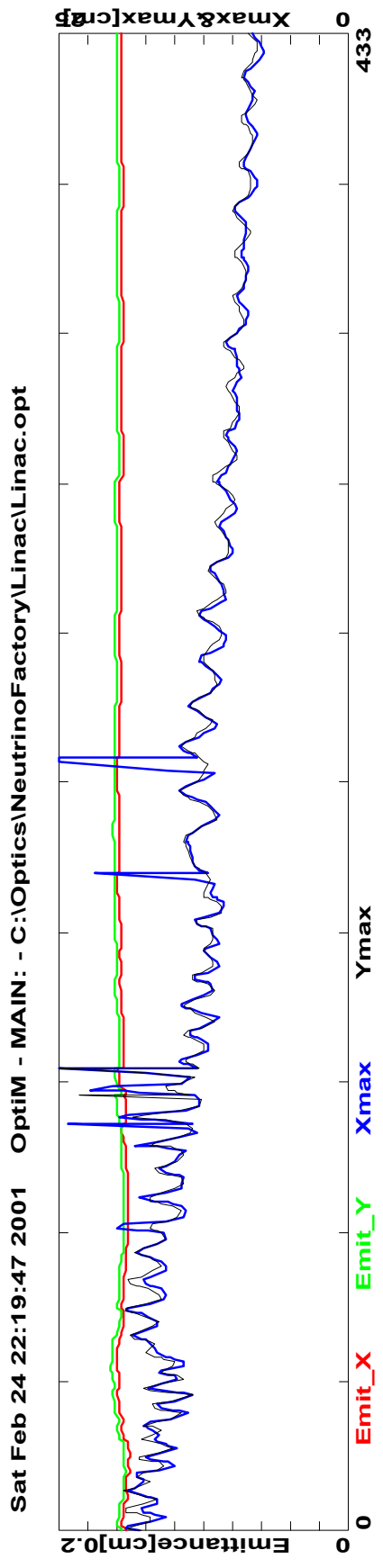
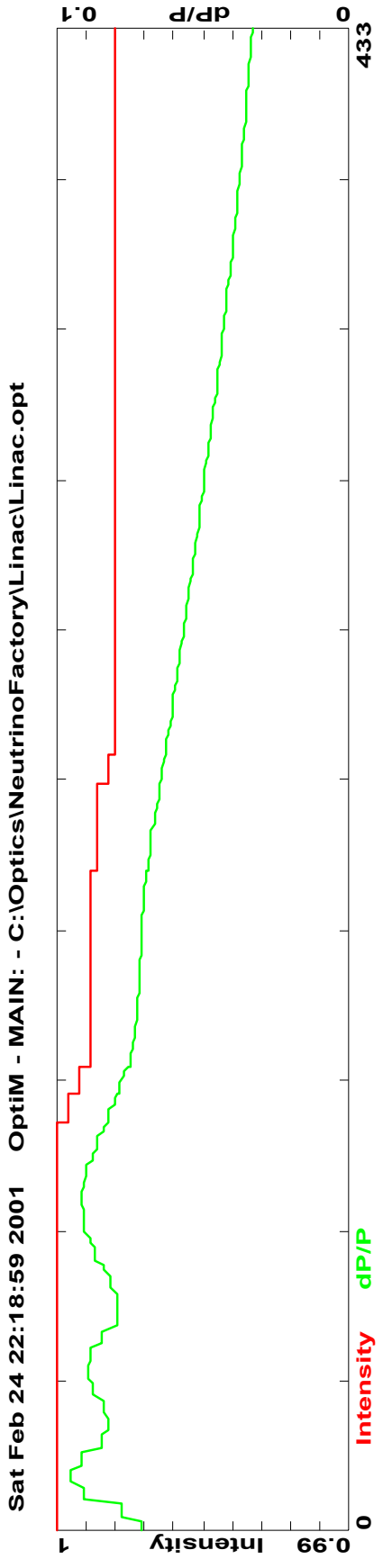


Figure 18. Dependence of beam intensity, rms momentum spread, beam emittances and beam envelopes along the linac.